JOURNAL OF SPACECRAFT AND ROCKETS
Vol. 43, No. 2, March–April 2006

Free-Flight Testing in Support of the Mars Science Laboratory Aerodynamics Database

Jeff Brown,* Leslie Yates,† David Bogdanoff,‡ and Gary Chapman§
Eloret Corporation, Moffett Field, California 94035
and
Mark Loomis¶ and Tim Tam**
NASA Ames Research Center, Moffett Field, California 94035

An extensive ballistic range test program to study the aerodynamic characteristics of two possible configurations for the Mars Science Laboratory entry vehicle is presented. Testing focused primarily on static and dynamic aerodynamic coefficients, in the pitch plane, for a tabbed geometry flying supersonically in carbon dioxide. Limited data were also obtained for tabbed models in air and for axisymmetric models, similar to the Viking/Pathfinder forebody shape, at supersonic and hypersonic Mach numbers in CO_2. Innovations in testing and data-reduction procedures that enhanced experimental capabilities and reduced data uncertainties are described. In CO_2, the tabbed configuration was dynamically stable, in pitch, for all trim angles and Mach numbers tested. Preliminary data showed the same vehicle to be unstable in air, suggesting the possibility of a significant gas-composition effect on pitch damping. In general, the experimental data agreed well with pretest computations.

Nomenclature

C_D	=	drag-force coefficient
C_L	=	lift-force coefficient
C_m	=	pitching-moment coefficient
$C_{m_q} + C_{m_\dot{\alpha}}$	=	pitch damping
C_N	=	side-force coefficient
C_n	=	yawing-moment coefficient
M	=	Mach number
Re	=	Reynolds number
Re_D	=	Reynolds number based on diameter
α	=	angle of attack
α_{rms}	=	rms angle of attack, $\sqrt{\frac{1}{N}\sum_{i=1}^{N}\alpha_i^2}$
β	=	yaw angle
σ	=	standard deviation

Introduction

THE Mars Science Laboratory (MSL) represents the first in a new generation of Mars missions for which the required landing accuracies will be an order of magnitude greater than those for Viking, Mars Pathfinder (MPF), and the Mars Exploration Rovers (MER): the first-generation Mars lander missions. The tighter MSL landing requirement calls for precision in guidance, navigation, and control during all phases of atmospheric entry. Bank modulation, which exploits the lift force on the entry vehicle (EV), will be used for active control during entry. Preliminary trajectory simulations[1] accounting for uncertainties in entry conditions demonstrated the need for a lift-to-drag ratio (L/D) on the order of 0.25. A key input to these six-degree-of-freedom (DOF) simulations is the aerodynamic database of the EV, the set of functions defining its aerodynamic coefficients in terms of geometric, atmospheric, and flow parameters. Large uncertainties in this database significantly reduce the accuracy of the six-DOF simulations. Therefore, the static (force and moment coefficients) and dynamic (pitch and yaw damping) aerodynamics of the EV must be well defined to ensure successful design of the EV's trajectory and its guidance control algorithm. Accurate knowledge of the supersonic aerodynamics, in particular, is required for successful supersonic parachute deployment, a critical and complex process for which the EV must be oriented correctly.

The MSL EV breaks from Viking/MPF/MER heritage in some key ways. First, a nonaxisymmetric forebody design is being considered. Second, the backshell geometry is different. And third, unlike MPF and MER, it will fly a lifting trajectory. For these reasons, extensive experimental data are needed to complement and validate the computational fluid dynamics (CFD) being used to generate most of the MSL aerodynamics database.

The Hypervelocity Free Flight Facility (HFFF), or ballistic range, at the NASA Ames Research Center (ARC), possesses unique capabilities that allow it to contribute significantly to the MSL aerodynamics database effort. The primary objective of the testing effort described in this paper was to determine the pitch-plane aerodynamics, with uncertainties, for two candidate EV configurations in the Martian atmosphere: static coefficients to validate CFD results and dynamic coefficients at the design trim angle for stability criteria.

Test Facilities and Method

ARC Ballistic Range (HFFF)

A schematic representation of the ballistic range, configured for supersonic testing, appears in Fig. 1. The range is composed of the powder gun, receiver tank, test section, and model catcher. For hypersonic testing, which employs a two-stage light-gas (H_2 or He) gun to launch the model, a pump tube is located upstream (to the right) of the gun.

The flight model is packaged in a cylindrical sabot, which is made of a lighter material and cut into four fingers, and loaded into the

Received 14 January 2003; revision received 1 August 2004; accepted for publication 1 February 2005.

*Senior Research Scientist, Reacting Flow Environments Branch, NASA Ames Research Center.
†Subcontractor; also Vice President, AerospaceComputing, Inc., Mountain View, CA 94303. Senior Member AIAA.
‡Senior Research Scientist, Reacting Flow Environments Branch, NASA Ames Research Center. Associate Fellow AIAA.
§Senior Research Consultant. Fellow AIAA.
¶Research Scientist, Reacting Flow Environments Branch. Senior Member AIAA.
**Research Scientist, Reacting Flow Environments Branch; currently Project Engineer, Cisco Systems, Inc., San Jose, CA 95134. Associate Fellow AIAA

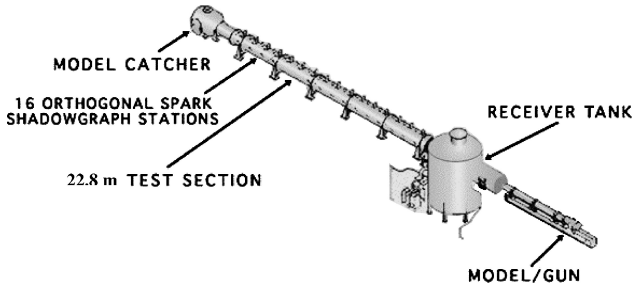

Fig. 1 NASA Ames HFFAF.

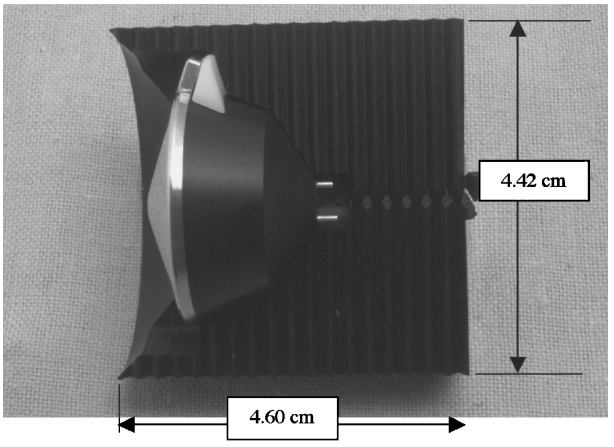

Fig. 2 MSL tabbed ballistic range model, with Teflon wedge, in half-sabot.

upstream end of the gun. In Fig. 2, a model resting in a half-sabot is shown with the nominal sabot dimensions. As the launch package is loaded, the tightness of its fit in the gun is gauged. This is because, along with the desired test velocity and the launch-package mass, the tightness of fit in the barrel is used to determine, from historical plots of HFFF launch conditions, the proper mass of gunpowder for the shot.

The launch process is illustrated in Fig. 3. When the gunpowder is ignited, combustion gases directly accelerate the launch package through and out of the gun barrel. (In light-gas gun operation, for hypersonic velocities, the burning gunpowder first accelerates a large, high-density polyethylene cylinder that greatly compresses the light gas inside the pump tube, which in turn forces the launch package through the barrel.) Once the launch package leaves the gun and begins to fly freely in the receiver tank, aerodynamic forces acting against the inclined leading surface of the sabot begin to peel it away from the model. A few meters downstream, the sabot fingers are stopped in the receiver tank by a conical, steel stripper, while the free-flying model passes into the test section through a hole in the center of the stripper. The models and sabots suffer impact damage at the end of their flights and are not reused.

The test section, shown in Fig. 4, possesses 16 optical stations spaced 1.524 m apart. (This spacing was more than adequate to capture the oscillation frequency of the MSL models, a function of the models' mass and aerodynamic properties, the latter being estimated by CFD.) Each station has two orthogonal pairs of windows, allowing both side and top views of the model. As the model traverses each station, it passes through a photo beam, which triggers a high-intensity light emission from two spark sources: one on top of the test section and one on the side. Each spark emission is reflected and collimated by a spherical mirror and passed through the test section. On the opposite side it is focused through a high-speed (30–40 ns) Kerr cell electro-optical shutter and expanded onto a 20×25 cm film plane. Along with the high-intensity spark sources, the Kerr cells are activated at each station when the model crosses the photo beam, and a highly accurate, elapsed-time clock, which was started at the time of powder ignition, is stopped.

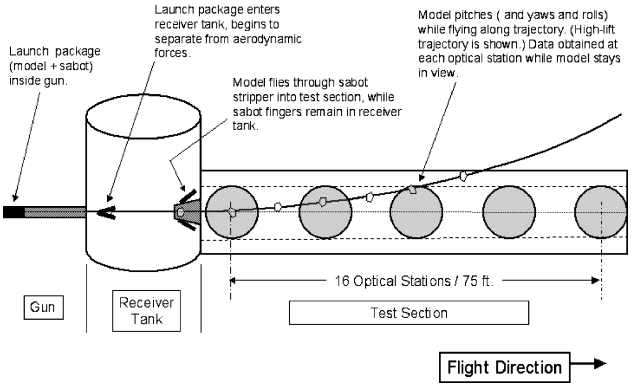

Fig. 3 Illustration of model launch process.

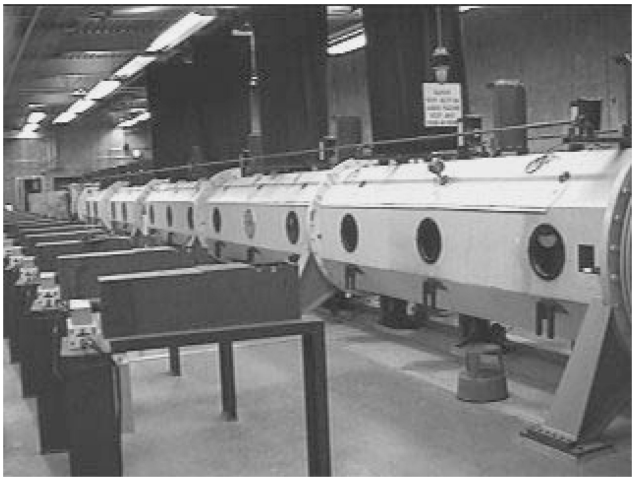

Fig. 4 HFFAF test section, with Kerr cells and film boxes.

The HFFF has a long heritage of supporting aerodynamics databases for space exploration programs, including Apollo, Viking, Pioneer Venus, AFE, and Galileo.[2–5] For these types of programs, it offers unique capabilities compared to wind tunnels and other aerodynamics ranges. As a free-flight facility with a quiescent medium, it has no stings, mounts, or freestream and wall turbulence, all of which can greatly compromise data quality. The HFFF also allows both Mach and Reynolds numbers to be varied independently over significant ranges. Test speeds range from hypersonic to subsonic. The gas pressure in the test section can be regulated between near vacuum and atmospheric. Thus, much of the Reynolds-number range between actual atmospheric entry and parachute deployment can be achieved.

Perhaps the most unique capability of the HFFF is being able to test in virtually any gas. Most wind tunnels and ballistic ranges only use air as the test medium. Yet, it is not well understood how the aerodynamics of a vehicle flying in air differ from those of the same vehicle flying in another gas. The ability to use different test gases in the HFFF allows simulation of the MSL EV in a representative CO_2 atmosphere, thereby eliminating the test gas as a source of uncertainty in the aerodynamic coefficients to be applied in flight.

During the test program, a technique of slanting the powder gun was developed to keep the flight of moderately high-lift models in view longer. This new capability adds greatly to the scope of testing that can be performed in the HFFF. Its motivation and application are described in greater detail in the following section.

Flight-Test Models and Sabots

Models of two external shapes were tested: the baseline, axisymmetric (M1) geometry, and the 20-deg tabbed (M3) configuration. The actual MSL EV will fly a lifting trajectory and therefore must trim at a nonzero angle of attack. The tab is being considered as a possible mechanism to effect the necessary trim angle without requiring

Table 1 Inertial properties of ballistic range models

Model	Mass, g	Xcg, cm	Ycg, cm	Zcg, cm	Ixx, g-cm^2	Iyy, g-cm^2	Izz, g-cm^2
			Axisymmetric geometry				
M1	22.559	0.653	0.000	0.000	18.117	13.128	13.128
M1A	25.166	0.662	0.000	0.078	21.010	15.245	14.216
			Tabbed geometry				
M3A	29.438	0.673	0.000	0.075	25.705	17.734	17.594
M3Ax	26.842	0.927	0.000	0.080	25.748	19.410	18.580
M3B	30.121	0.672	0.000	0.062	26.540	18.150	17.079
M3C	29.889	0.668	0.000	0.012	26.473	18.459	16.280

Note: Nominal diameter and length were 3.05 and 2.21 cm, respectively, for all models. Xcg was measured from model nose, along its axis. Ycg and Zcg are perpendicular to the model axis, in the yaw and pitch directions, respectively.

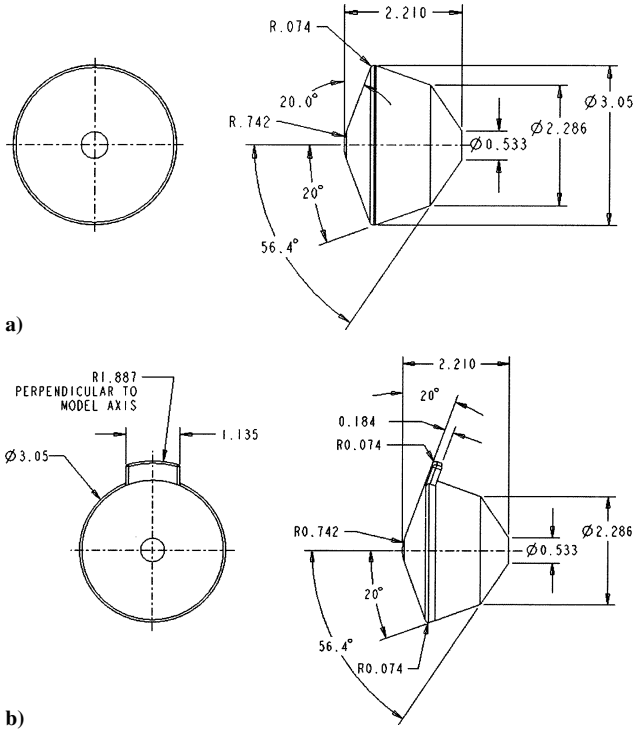

Fig. 5 Dimensions (in centimeters) of MSL ballistic range models: a) M1 (axisymmetric) geometry and b) M3 (tabbed) geometry.

the large radial c.g. offset needed by the baseline EV. Drawings of the two geometries are shown in Figs. 5a and 5b; dimensions are in centimeters. Both model types had a metallic 70-deg sphere-cone forebody and a biconic (20-/56.4-deg) aftbody made out of acrylonitrile butadiene styrene (ABS) or, in one specific case, the M3Ax, aluminum.

The nominal inertial properties for all of the models tested are presented in Table 1. Two versions of the axisymmetric geometry were tested: the simple M1 had an on-axis c.g. and was designed to fly at 0 deg α, while the M1A's radial c.g. offset caused the model to trim at an approximate α of 15 deg, producing lift. The M1 and the M1A were both tested hypersonically and supersonically.

In addition to the fore- and aftbody, the M3-configuration models also had a brass tab collar. An exploded view appears in Fig. 6. This three-part construction gave the operational advantage of only having to modify the tab collar in order to change the radial c.g. offset and, therefore, the trim angle (α trim) for the model. Tabbed models with three nominal trim alphas (and model designations) were tested: 0 deg (M3A), 4 deg (M3B), and 14 deg (M3C). A special case of the M3A model, the M3Ax, was designed to place the c.g. aft by roughly 10% of the model diameter. It employed aluminum as the fore- and aftbody material to accomplish the desired axial c.g. shift.

For all tabbed models, two 0.076-cm-diam roll pins were bonded into the flat base section at the 12 and 6 o'clock positions, 0.381 cm apart, to enhance roll-angle determination (Fig. 6). The combined cross-sectional area of the pins was less than 10% that of the 0.533-cm-diam base, and only 0.25% that of the whole model aftbody. They are not believed to have significantly affected the models' aerodynamic behavior. All models were launched inside a four-piece, serrated sabot made of ABS plastic.

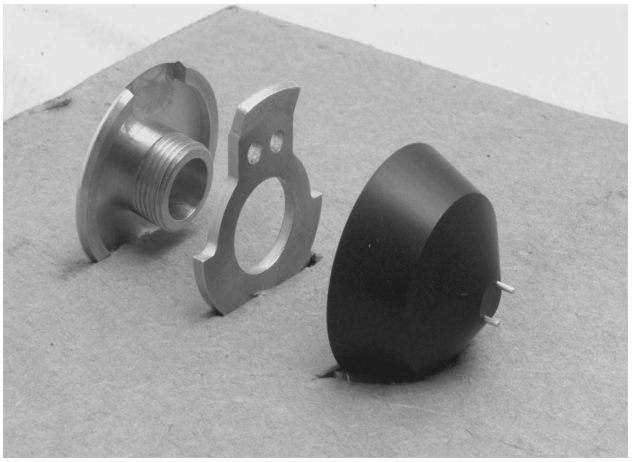

Fig. 6 Three-part construction of the tabbed (M3) test model.

Pretest Predictions

Computational predictions of the steady-state aerodynamic forces on the M1 and M3 configurations were made using the General Aerodynamics Simulation Program (GASP).[6] GASP has been used extensively at ARC for aerodynamics and heat-shield sizing applications, for both planetary[7,8] and transatmospheric[9] EVs. The code solves the full Navier–Stokes equations, including species equations for thermochemistry, with a finite volume spatial discretization.

Typically, for predictions of flight at Mars, the atmosphere of which is 96.85% CO_2 and 3.15% N_2, an eight-species (N_2, O_2, NO, N, O, CO_2, CO, C) finite-rate chemistry model with the Park-94[10] reaction rates is used. This same thermochemical model was used for the hypersonic ballistic range calculations, for consistency, but it was assumed that the freestream composition of the test gas was pure CO_2. At the supersonic test condition, the velocity is too low for significant dissociation to occur. Therefore, to speed up the computation, a simplified one-species (CO_2) model was used. At the surface, no-slip, constant-temperature ($T = 300$ K) conditions were applied—the model heats up only marginally during flight in the ballistic range—and a laminar boundary layer was assumed. Full body, O-type grids were generated using the Gridgen[11] software package and adapted to the flow with the Self Adaptive Grid CodE (SAGE)[12] grid-adaptation package. A grid-convergence study demonstrated that 65 axial, 33 circumferential, and 65 normal points were sufficient to model the aerodynamics.

According to predictions, the baseline MSL EV needs to trim at $\alpha = 15$ deg to fly with the required L/D of 0.25. Therefore, for the ballistic range tests supersonic ($M = 2.5$) aerodynamic coefficients

were predicted for α from 0 to 20 deg, and for hypersonic ($M = 18.7$) predictions α ranged from 0 to 15 deg. The reference areas used for the M1 and M3 geometries were the same; they were based on the forebody not including the tab. The pitching moment was referenced to a c.g. location of $(x, y, z) = (0.660,0,0)$ cm, where x is measured along the model axis from the nose and y and z are orthogonal to the axis, z being in the positive pitch direction.

Note that the primary purpose of these computations was to support the experimental design process by predicting a model's approximate flight trajectory through the range as a function of nominal mass properties and flight conditions. Because it was not an aim of this study to develop or validae CFD, no attempt was made following the test to refine the computations based on the actual test parameters.

Hypersonic Testing

The test program began with hypersonic shots, from the 3.81-cm light gas gun, of the M1 and M1A models into CO_2. The parameters for the shots that yielded the most useful data appear in Table 2. Nominal test-section pressures of 75 and 100 torr were used.

In actual flight, any EV experiences perturbations in its pitch angle. Therefore, designers not only need to know a vehicle's aerodynamics at its design trim angle, but over a range of angles encompassing it. To obtain this information from free-flight tests, a given geometry is flown multiple times at the same nominal test conditions (i.e., M, Re), but with varying perturbation amplitude, or rms α. Within a given project's time and cost constraints, the accuracy and reliability of the measured data can be increased by testing at more α rms values and making more shots for each value. For the M1 models, and the tabbed models that trimmed at much smaller angles than the MSL EV design trim α of 15 deg, these perturbations were needed to ensure that each model's range of motion passed through that design trim value.

To impart the desired pitch oscillation, a sheet of paper was mounted between the sabot stripper and test section, below the facility axis, for each shot. The paper "kicked" the lower part of the model as it flew into the test section, generating a pitch oscillation. A larger oscillation (α rms) would result from using heavier paper or mounting the paper farther off axis. This technique was also used in the supersonic testing of the M1 configuration; however, a different approach, discussed later in the paper, was employed for the M3 tests.

The same method of achieving pitch can be used to achieve yaw. However, the current test program focused primarily on establishing the aerodynamics in the pitch plane (i.e., drag, lift, pitching moment, and, for the M3 geometry, pitch-damping coefficients) as a function of the angle of attack. No attempt was made to vary β rms.

Supersonic Testing

Table 3 shows the test parameters for supersonic shots made with the M1 and M1A models from the 4.45-cm powder gun. The test gas was CO_2 at nominal pressures of 110 and 40 torr for the M1 and M1A tests, respectively. The lower pressure condition was selected to reduce the lift force on the M1A and, consequently, increase the number of stations over which the model would stay in view, thereby allowing more accurate measurements of the static coefficients. However, lowering the test pressure also reduces the frequency of the model's pitch oscillations, which resulted in insufficient data for determining the dynamics. This problem was solved by slanting the gun, which is discussed in the section on Data Acquisition, Processing, and Analysis.

Table 4 shows the test matrix and shot parameters for the tabbed models. The shots were, again, made from the 4.45-cm powder gun. Most shots were made in CO_2, but some tests in air were also performed to gain preliminary information on whether the change in test gas would significantly affect the measured aerodynamics, particularly pitch damping.

Table 2 Hypersonic test conditions for M1 and M1A

Model	Shot no.	V, m/s	M	Re_D	α_{rms}, deg	α_{trim}, deg
M1	2234	4730	17.59	$2.30E+06$	5.5	0.0
M1	2236	5040	18.71	$1.88E+06$	8.3	0.0
M1A	2238	5139	19.11	$1.91E+06$	11.6	11.7

Table 3 Supersonic test conditions for M1 and M1A

Model	Shot no.	V, m/s	M	Re_D	α_{rms}, deg	α_{trim}, deg
M1	2242	925.7	3.44	$0.496E+06$	3.7	0.0
M1	2243	677.4	2.52	$0.364E+06$	3.8	0.0
M1	2246	823.5	3.07	$0.447E+06$	18.3	0.0
M1	2248	671.2	2.50	$0.360E+06$	6.2	0.0
M1A	2244	467.1	1.74	$0.092E+06$	29.5	19.0
M1A	2247	939.5	3.50	$0.187E+06$	17.9	18.4
M1A	2249	857.3	3.19	$0.180E+06$	19.3	19.1

Table 4 Supersonic test conditions for M3 models

Model	Shot no.	V, m/s	M	Re_D	α_{rms}, deg	α_{trim}, deg
M3A	2251	697.3	2.60	$0.382E+06$	25.9	2.2
M3A	2252	721.4	2.69	$0.390E+06$	18.0	1.2
M3A	2253	734.8	2.74	$0.412E+06$	19.5	1.3
M3A	2255	680.7	2.54	$0.371E+06$	9.1	−0.9
M3A	2259	718.4	2.69	$0.391E+06$	15.8	1.0
M3A	2254	908.2	3.40	$0.501E+06$	21.9	1.9
M3A	2257	956.0	3.56	$0.517E+06$	15.9	1.5
M3A	2258	995.0	3.71	$0.541E+06$	7.4	0.7
M3A	2264	1031	3.84	$0.556E+06$	21.6	0.9
M3A	2267	1046	3.89	$0.570E+06$	20.1	1.0
M3Ax	2260	722.5	2.70	$0.398E+06$	8.4	0.5
M3Ax	2261	676.4	2.53	$0.368E+06$	21.5	1.6
M3Ax	2263	731.6	2.73	$0.394E+06$	28.4	2.8
M3Ax	2266	706.1	2.64	$0.383E+06$	19.8	1.5
M3B	2262	651.8	2.44	$0.356E+06$	18.6	4.5
M3B	2265	717.3	2.68	$0.387E+06$	11.0	4.1
M3B	2268	748.8	2.78	$0.404E+06$	20.1	4.1
M3B	2269	781.8	2.91	$0.421E+06$	14.4	4.2
M3C[a]	2271	737.9	2.75	$0.403E+06$	16.6	14.6
M3C	2273	769.4	2.86	$0.415E+06$	19.1	14.7
M3C	2274	745.9	2.78	$0.402E+06$	15.5	14.3
M3C	2275	723.0	2.69	$0.387E+06$	14.7	14.4
M3C[a]	2276	922.3	2.67	$0.406E+06$	13.8	13.8
M3C[a]	2277	898.8	2.61	$0.394E+06$	14.8	14.1
M3C	2279	714.5	2.66	$0.382E+06$	18.4	11.7
M3C	2281	772.3	2.87	$0.412E+06$	20.4	13.7

[a]Test gas was air or (for no. 2271) CO_2/air mix.

Tables 2–4 present average values for velocity, Mach number, and Reynolds number. Most of the models lost on the order of 10% in velocity between optical stations 1 and 16. The analysis, described next, assumes that the aerodynamics are constant functions of Mach number over that small Mach-number range.

Initial shots of the M3 models revealed an unexpectedly large amplitude in the pitch oscillations. It was concluded to be the result of the high-pressure muzzle gases driving the upper part of the sabot into the back of the model tab as the launch package exited the gun and began to separate. As mitigation, a Teflon® wedge with a sloped backface (see Fig. 2) was used to support the tab against acceleration loads during launch and deflect the kick from the sabot immediately after the launch. Previously, the sabot had supported the tab directly. It was soon determined that by varying the slope on the backface of the wedge it was possible to prescribe for each model the approximate magnitude of its in-flight pitch oscillations. A larger slope, that is, larger angle at the top of the wedge, yielded a smaller α rms. This technique proved to be more accurate and reliable in controlling α rms than kicking the model with paper, and it was used for the remainder of the program.

Data Acquisition, Processing, and Analysis

The purpose of the current test was to use free-flight data from a number of MSL models to develop expressions for aerodynamic coefficients, like those in Table 5, which could be used in vehicle control algorithms.

Table 5 Equations for aerodynamics

Coefficient	Coefficient expansion	3-σ uncertainty
	Axisymmetric geometry (M1), hypersonic	
C_D	$1.704 - 4.3\sin^2\alpha$	$0.004 + 0.3\sin^2\alpha$
C_L	$-1.49\sin\alpha$	$0.07\sin\alpha$
C_m	$-0.128\sin\alpha$	$0.002\sin\alpha$
	Axisymmetric geometry (M1), supersonic	
C_D	$1.619 - 1.83\sin^2\alpha$	$0.002 + 0.03\sin^2\alpha$
C_L	$-1.56\sin\alpha + 2.1\sin^3\alpha$	$0.03\sin\alpha + 0.4\sin^3\alpha$
C_m	$-0.107\sin\alpha - 0.084\sin^3\alpha$	$0.002\sin\alpha + 0.010\sin^3\alpha$
	Tabbed geometry (M3), supersonic, $M = 2.6$[a]	
C_D	$1.689 + 0.057\sin\alpha - 1.85\sin^2\alpha$	0.03
C_L	$-0.005 - 1.77\sin\alpha - 0.021\sin^2\alpha + 2.23\sin^3\alpha$	0.040
C_N	$-1.1\sin\beta$	$0.2\sin\beta$
C_m	$0.0401 - 0.136\sin\alpha - 0.0381\sin^3\alpha$	0.003
C_n	$-0.129\sin\beta$	$0.005\sin\beta$
	Tabbed geometry (M3), supersonic, $M = 3.6$	
C_D	$1.717 - 0.008\sin\alpha - 2.16\sin^2\alpha$	0.03
C_L	$-0.03 - 1.74\sin\alpha + 3.02\sin^3\alpha$	0.035
C_N	$-1.3\sin\beta$	$0.2\sin\beta$
C_m	$0.0371 - 0.124\sin\alpha - 0.092\sin^3\alpha$	0.003
C_n	$-0.14\sin\beta$	$0.01\sin\beta$

[a]c.g. located at $(x, y, z) = (0.671, 0, 0)$ cm.

For every model shot in the HFFF, side- and top-view shadowgraphs were taken at each of the 16 optical stations using 20×25 cm, Kodak Tmax 400 film. Vertical and horizontal (catenary) fiducial wires at each optical station, which appear in the shadowgraphs, provided a basis for determining the model's instantaneous position and attitude. For the M1A and tabbed models, pins were attached to the flat, rear surface to facilitate measurement of the instantaneous roll angle. The range pressure and temperature were recorded for each shot.

The shadowgraphs were digitized and initially reduced using the Comprehensive Aerodynamic Data Reduction System for Aeroballistic Ranges-1 (CADRA1) image processing and trajectory measurement program. The code CADRA1 is an extension of the public-domain application National Institutes of Health Image, with the following additional features: object (model, fiducial wires, etc.) identification; the ability to employ both least-squares and centroid methods for measuring object position and orientation with subpixel resolution; and, trajectory identification. During image processing, the position and orientation of the model and fiducial images in each shadowgraph were measured. The program then transformed these image measurements to three-dimensional position and orientation (trajectory) data using a file containing the known locations of the fiducial wires in the fixed facility coordinate system.

The aerodynamic coefficients are determined from the three-dimensional trajectory information. The drag force slows a model as it flies down the range. Lift causes it to swerve. The pitching and yawing moments cause the model to oscillate in the pitch and yaw planes. And the pitch and yaw damping serve either to increase or decrease the oscillation amplitudes. For trimmed models flying in the range, the deceleration and swerve rates can be obtained from just a few sequential optical stations. The frequencies of pitch and yaw oscillations can be determined from little more than a half-cycle of motion. Therefore, relatively few data are needed from each shot to identify the static coefficients of drag, lift, and moment.

To obtain the vehicle dynamics, such as pitch and yaw damping, however, enough information must be available to measure both the trim angle and the change in oscillation amplitude. Generally, to do this accurately, two cycles of motion, with at least six to seven points per cycle, are required. During testing of models flying at low trim angles (therefore, low lift), the trajectory stayed close to the test-section axis, the model stayed in view for all 16 optical stations, and the aforementioned criteria were met. However, for the highest trim (i.e., M1A and M3C) models, those closest to the actual MSL EV design trim, the strong tendency was to lift out of view between 50 and 75% of the way down the range. Therefore, the required

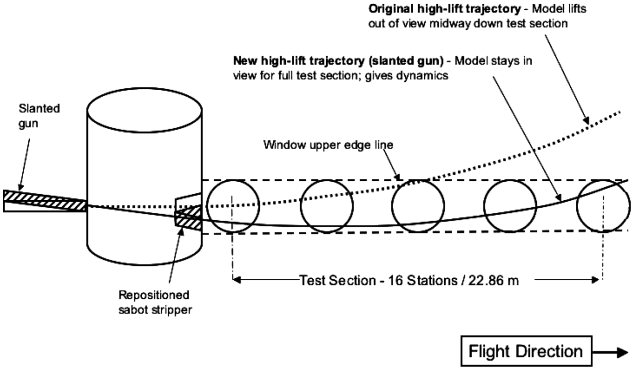

Fig. 7 Slanting the gun to accommodate high-lift trajectories.

number of cycles with sufficient resolution to allow measurement of dynamics could not be recorded. This problem was overcome by tilting the gun so that the parabolic path of the model reached its minimum elevation partway down the test section, rather than at the gun muzzle, and the model stayed in view for the full 16 stations. The process is depicted in Fig. 7.

The quality of the aerodynamic results also depends on the accuracy of the trajectory measurements. During testing, modifications that improved the accuracy of the trajectory measurements were implemented in CADRA1. First, the angle measurement capability for blunt bodies was augmented by combining centroid and straight-edge techniques. This combination of techniques was particularly helpful for the hypersonic data, where, initially, the very small shock stand-off distances made the front surface of the model difficult to define, resulting in undesirably large errors in the estimations of the pitch and yaw angles. By using only the well-defined aft surfaces of the model for angle measurements, errors were reduced significantly. Second, methods for identifying the roll pin locations, and therefore the roll measurements, were enhanced. Reducing the errors in the roll measurements was particularly important for separating the pitch and yaw motions of the tabbed configuration.

The trajectory measurements were reduced to aerodynamic coefficients using the CADRA2 program. With CADRA2, coefficients are determined using a least-squares, differential correction procedure, which adjusts the aerodynamic parameters and initial conditions until a best least-squares fit of the trajectory measurements is obtained. Two versions of CADRA2 were used. For the M1 and M1A models, a version with aerodynamic functions suitable for

axisymmetric geometries was used. For the tabbed models, a version of CADRA2 was used that would handle airplane-like configurations, that is, the aerodynamics in the pitch and yaw planes are allowed to differ.

The trajectory measurements were reduced to the final aerodynamic information in three steps. First, the individual runs were analyzed by using linear aerodynamics. The resulting single-fit data points represent average values of the coefficients that are valid for particular rms angles of attack, that is, those of the trajectories from which they were taken. Note that, in general, the drivers of nonlinear aerodynamics, such as variations in Mach number, oscillation amplitude, and c.g. location, are either small or absent for individual HFFF runs. Therefore, the use of linear aerodynamics was appropriate for this step.

In the second step, the single-fit data were plotted vs the rms angle of attack for the purpose of establishing any nonlinear trends and selecting the appropriate nonlinear aerodynamics math modeling functions. If the aerodynamics are linear in α, the single fits will fall on a straight line when plotted in this fashion. However, if there are nonlinearities, the data will define some type of curve, the shape of which provides information for selecting the proper nonlinear modeling functions.

For this series of tests, the nonlinear functions that were selected to model the coefficients for drag, lift, pitching moment, and pitch damping, for the axisymmetric geometry, are given in Eqs. (1a–1d), respectively:

$$C_D = C_{D_0} + C_{D_{\alpha^2}} \sin^2 \alpha \tag{1a}$$

$$C_L = C_{L_0} + C_{L_\alpha} \sin \alpha + C_{L_{\alpha^3}} \sin^3 \alpha \tag{1b}$$

$$C_m = C_{m_0} + C_{m_\alpha} \sin \alpha + C_{m_{\alpha^3}} \sin^3 \alpha \tag{1c}$$

$$C_{m_q} + C_{m_{\dot{\alpha}}} = \text{const} \tag{1d}$$

For the tabbed configuration, the selected nonlinear functions for drag, lift, normal force, pitching moment, yawing moment, and pitch damping are represented by Eqs. (2a–2f), respectively:

$$C_D = C_{D_0} + C_{D_\alpha} \sin \alpha + C_{D_{\alpha^2}} \sin^2 \alpha \tag{2a}$$

$$C_L = C_{L_0} + C_{L_\alpha} \sin \alpha + C_{L_{\alpha^3}} \sin^3 \alpha \tag{2b}$$

$$C_N = C_{N_\beta} \sin \beta \tag{2c}$$

$$C_m = C_{m_0} + C_{m_\alpha} \sin \alpha + C_{m_{\alpha^3}} \sin^3 \alpha \tag{2d}$$

$$C_n = C_{n_\beta} \sin \beta \tag{2e}$$

$$C_{m_q} + C_{m_{\dot{\alpha}}} = \text{constant} \tag{2f}$$

In the third and final step, runs with similar c.g. locations and Mach numbers were analyzed simultaneously to obtain the true, largely nonlinear aerodynamics (also called *multifits*), which appear in Table 5. By simultaneously analyzing several runs with different angle-of-attack ranges, the accuracies of the nonlinear aerodynamic coefficients were improved.

Some of the process just described are illustrated in Figs. 8a and 8b. In Fig. 8a, three single-fit data points and the multifit, 3-σ error bounds are shown for the hypersonic lift coefficient of the axisymmetric geometry. The best multifit curve bisects the error bounds. The axis labels "avg" and "rms" do not normally pertain to multifits, which usually relate the instantaneous values of C_L and α. Here, however, so that a direct comparison of single fits and multifits could be shown, the latter is represented by a weighted average of C_L vs α rms. When C_L is linear, the weighted average vs rms angle is the same plot as that of the instantaneous values. However, that is not the case for a nonlinear coefficient.

The single fits in Fig. 8a lie very nearly on a line. Therefore, a linear form for C_L was chosen to simultaneously fit the three trajectories they represent. The best fit was provided by the expression found in Table 5. The single-fit point at α rms of 12 deg is from a lifting, M1A, model, not a nonlifting M1, and it flew out of view approximately halfway down the range. This resulted in fewer trajectory measurements and larger error bars for that point.

Table 6 Estimates of measurement errors

Case	Δx, cm	Δy, z, cm	$\Delta\theta$, ψ, deg	$\Delta\phi$, deg
M1-h	0.031	0.032	0.28	N/A
M1-s	0.020	0.049	0.31	N/A
M3	0.031	0.034	0.64	4.9

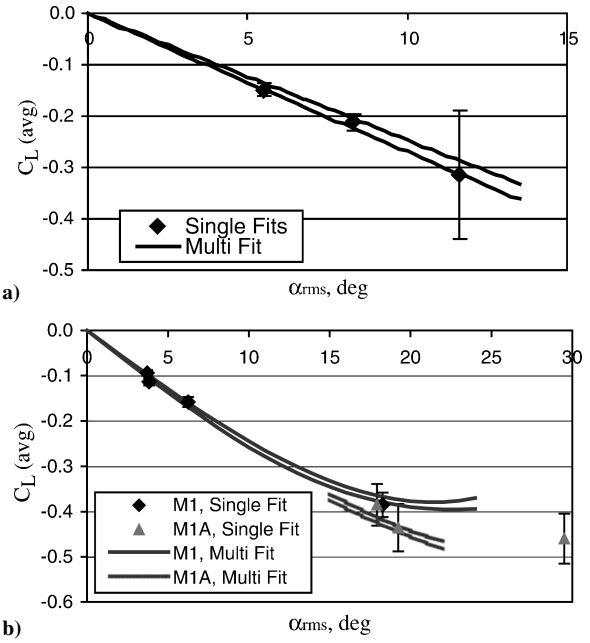

Fig. 8 Multifit vs single-fit lift coefficients for axisymmetric (M1) geometry: a) hypersonic and b) supersonic.

The single-fit and multifit (3-σ error bounds) supersonic lift coefficients for the axisymmetric geometry appear in Fig. 8b. Again, the multifit is a weighted average vs rms angle, not the usual instantaneous C_L vs α relation. Here we see that the single-fit data do not lie along a line. Thus, a nonlinear form for C_L was used to perform the multifits. Furthermore, at higher values of α, a different nonlinear equation than that used to fit the nonlifting, M1 trajectories is needed for the lifting, M1A multifits. The expression in Table 5 gives the best multifit for the M1 models, which, because they flew close to the tunnel axis, provided significantly more trajectory information than the M1As.

Errors and Uncertainties

Measurement Errors

The measurement errors for the model's instantaneous position and orientation are estimated by fitting calculated trajectories to the trajectory data points; quasi-linear aerodynamics are used for modeling the forces and moments. For single test runs with two cycles or less of motion and small losses in Mach number, the calculated trajectories using quasi-linear aerodynamics provide a reasonable simulation of the motion, and the residual errors provide a good estimate of an upper bound for the measurement errors.

The estimated upper bounds of the measurement errors for the M1 hypersonic, M1 supersonic, and M3 models are given in Table 6. Planetary entry vehicles like the MSL EV more closely resemble spheres than slender bodies, which makes their position and orientation more difficult to measure. Whereas the measurement errors for slender-body models of the same scale as the current, MSL models would typically be less than 0.005 cm for position and 0.1 deg for angles, the upper-bound errors shown in Table 6 are considerably higher.

Coefficient Uncertainties

Several factors affect the accuracy of the estimated aerodynamic coefficients, including the math models used for the coefficients, the range of angles and Mach numbers covered by the tests, and the measurement accuracy. First, the math models chosen to describe the coefficients must represent the functional behavior of the coefficients. Several methods can be used to identify the functional behavior, including CFD and quasi-linear analysis of the experimental data. When using the latter technique, quasi-linear coefficients for each test run are estimated, and the results plotted vs Mach number and rms angle of attack. The shapes of these curves guide the selection of the math models but not the values of the individual coefficients.

To determine accurate nonlinear coefficients over ranges of Mach numbers and angles, the test runs must span the ranges. If all test runs have similar Mach numbers and rms angles, quasi-linear aerodynamics will provide good fits to all of the data, and the nonlinear effects cannot be measured. However, if there are multiple runs with varying Mach numbers and/or rms angles, the quasi-linear models no longer provide reasonable fits; for example, for moment coefficients that are nonlinear in angle of attack, an average coefficient obtained for small-amplitude motions will not give good fits for large-amplitude motions.

Finally, the accuracy of the position and orientation measurements impacts the accuracy of the estimated aerodynamic coefficients. If these errors are large, large errors in the estimated coefficients are expected.

The estimated 3-σ uncertainties for the M1 configuration are obtained from the least-squares method and are proportional to the covariance matrix and residual errors.[13] The estimated uncertainty bounds for the M3 configuration encompass the 3-σ error bounds for the various configurations.

Any errors in modeling the aerodynamic coefficients are reflected in larger residual errors and, therefore, estimated uncertainties. Although it is possible that the math model might deviate enough from the actual shape of the corresponding aerodynamic coefficient that the actual value at a given angle or Mach number would not fall within the bounds of the estimated uncertainty, the nonlinear coefficient will give reasonable results for vehicles experiencing the angular motion and Mach-number ranges covered by the test.

For the hypersonic and supersonic cases, the impact of the 3-σ errors was tested by fixing one coefficient to its estimated value plus or minus its 3-σ uncertainty; all other terms were fitted using the parameter-identification software CADRA2. For the drag coefficient, this resulted in an 8–10% increase in the residual errors and a 3–5% increase for the moment and lift coefficients.

For the M3 models, the impact of the 3-σ errors was tested by fixing one coefficient to its estimated values plus or minus the 3-σ uncertainty identified in Table 5. For the drag coefficient, this resulted in a 200% increase in the residual errors; for the lift and moment coefficient, a 13–15% increase.

Results

M1 and M1A Configurations

The upper and lower, 3-σ error bounds in Figs. 9a–9d represent the nonlinear aerodynamics for the symmetric and trimmed configurations at hypersonic speeds. For each case, the best estimate falls between these two curves. Drag, lift, and pitching-moment coefficients are shown in Figs. 9a, 9b, and 9c, respectively. Figure 9d is the lift-to-drag ratio, constructed from the lift-and-drag curves. The nonlinear functions used to model the coefficients are given by Eqs. (1a–1d). Table 5 contains the best (multi-) fit values for those coefficients.

The CFD predictions are also shown in Figs. 9a–9d. For a few cases, both laminar and turbulent calculations were made. The effect of turbulence was found to be small, and most of the calculations were done only for laminar flow. For small angles of attack, the results agree within the error bounds. At larger angles, the results begin to differ by greater amounts. Part of this disagreement results from the lack of trajectory data for angles above 12–14 deg. Hence, the ballistic range curves are terminated at about 14 deg. The quasi-linear fits showed none of the nonlinear behavior exhibited by the CFD results for the pitching moment in Fig. 9c. To verify this would have required additional work beyond the scope of this study, including additional testing at angles where there are differences in the CFD and ballistic range results, refinement of the CFD solutions, and comparison to wind-tunnel results. However, the estimated coefficients reproduce the small-amplitude motions.

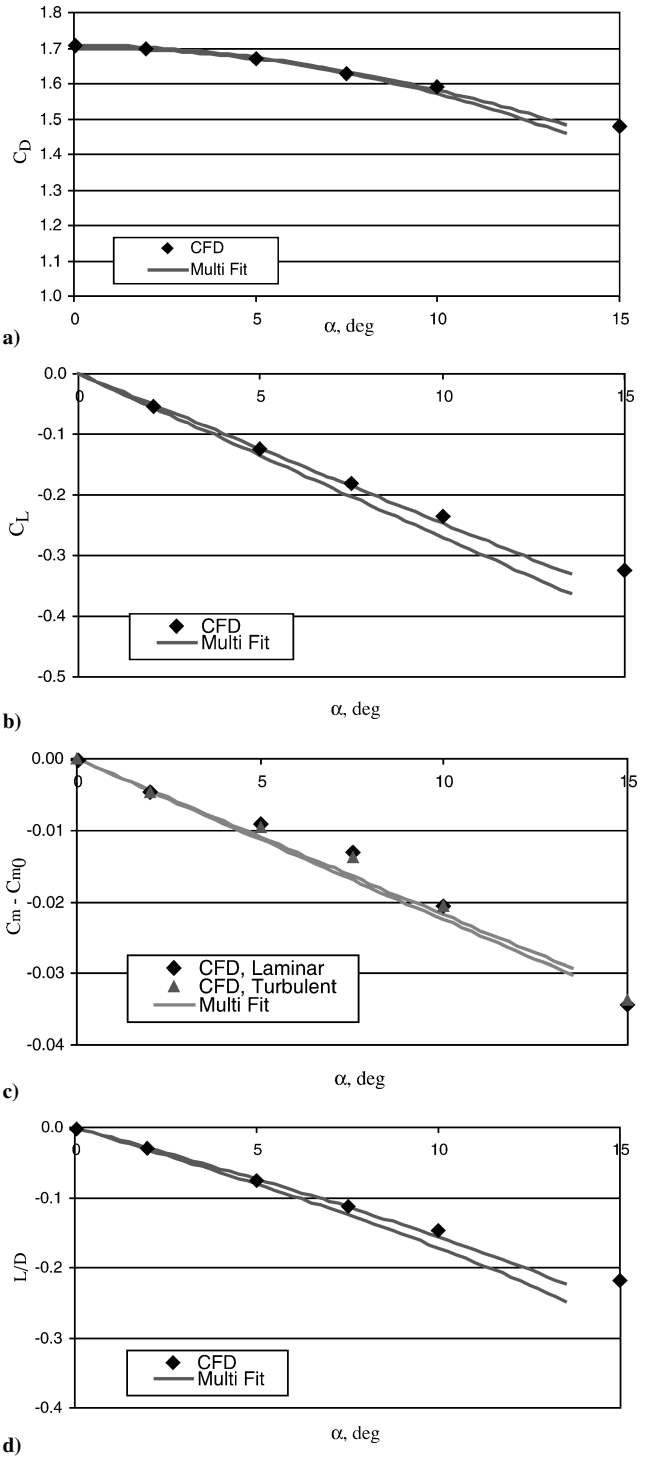

Fig. 9 Pretest CFD vs experiment for axisymmetric (M1) geometry in hypersonic flight: a) drag-force coefficient, b) lift-force coefficient, c) pitching-moment coefficient, and d) lift-to-drag ratio.

Similar results for the symmetric and trimmed configurations at supersonic speeds are shown in Figs. 10a–10d. There were many more tests at this condition; hence, the 3-σ error bounds are much smaller. Tests were also conducted at higher angles of attack, and the curve fit is made to nearly 25 deg. Again, CFD results are shown for

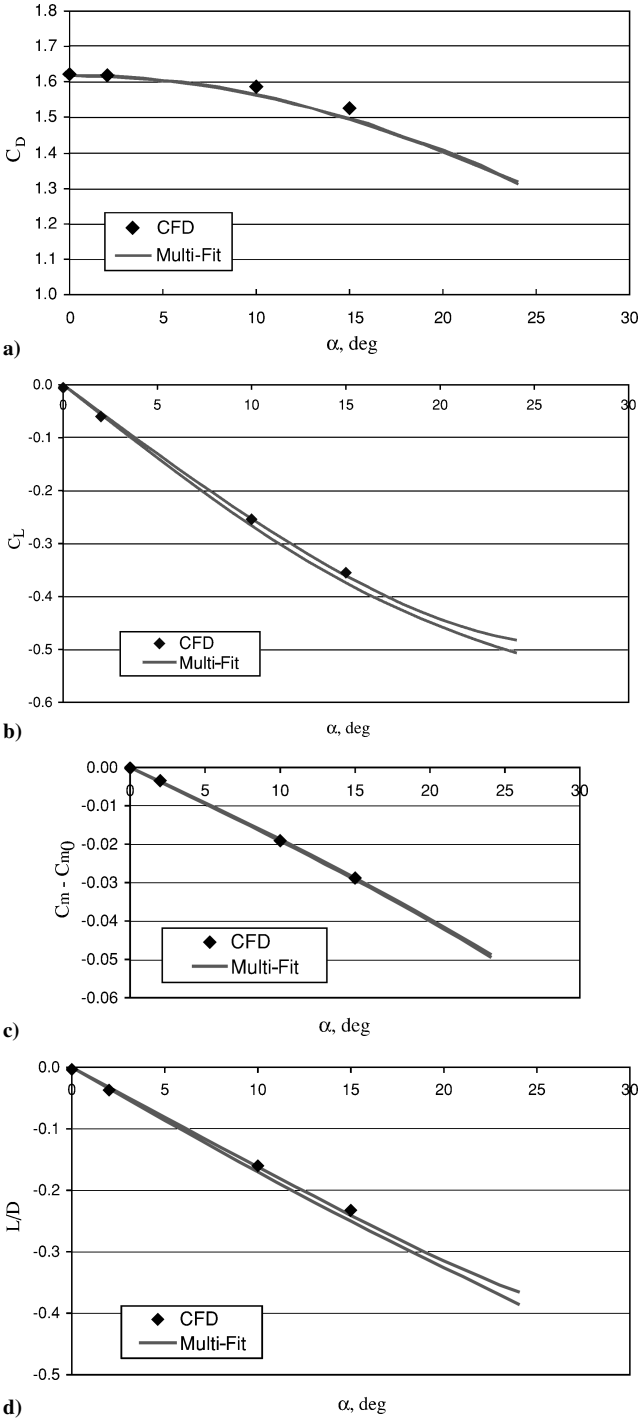

Fig. 10 Pretest CFD vs experiment for axisymmetric (M1) geometry in supersonic flight: a) drag-force coefficient, b) lift-force coefficient, c) pitching-moment coefficient, and d) lift-to-drag ratio.

comparison. The aerodynamics are more nonlinear in the supersonic regime than at hypersonic speeds. Also, the agreement between CFD and the ballistic range results is excellent, out to the extent of the CFD results.

Tabbed (M3) Configurations

The coefficients for drag, lift, pitching moment, and the lift-to-drag ratio for the tabbed geometry are shown in Figs. 11a–11d, respectively. Again, the data are shown as 3-σ error lines, and the corresponding CFD points are given. Here, the L/D predicted by CFD appears to have a slightly lower slope compared to the ballistic range data. Note that the trim angles in Tables 2–4 were calculated

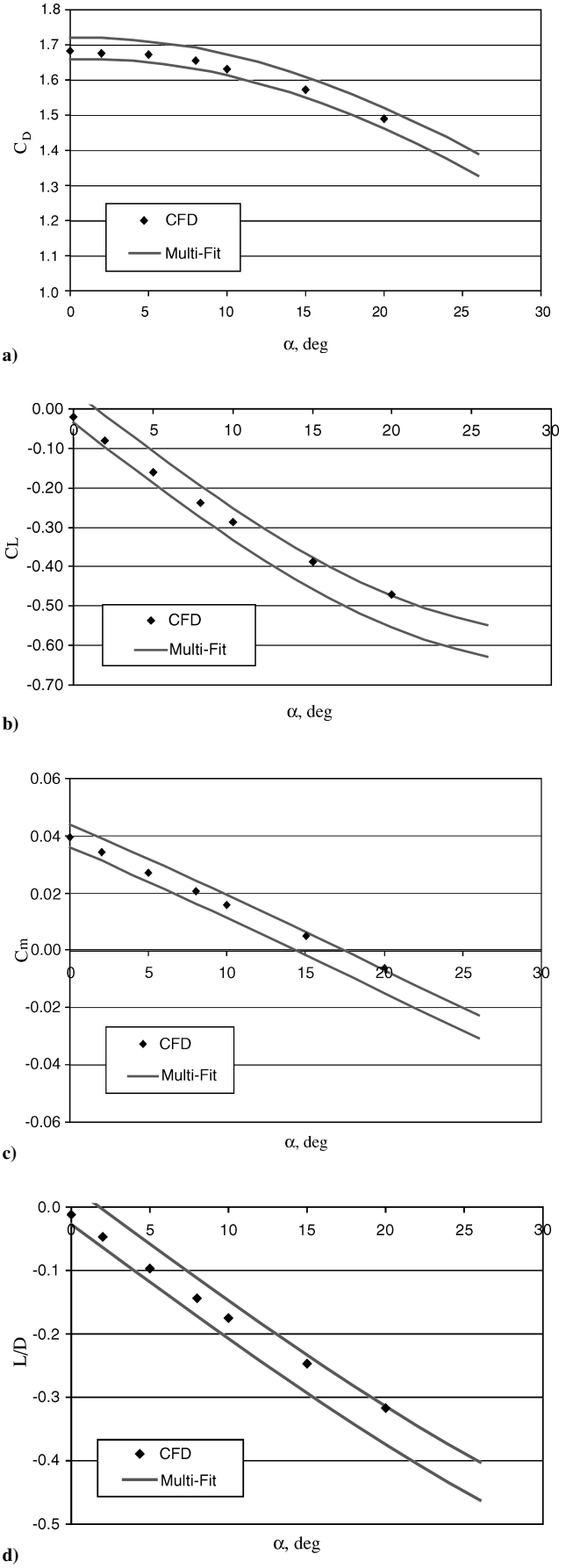

Fig. 11 Pretest CFD vs experiment for tabbed (M3) geometry in supersonic flight: a) drag-force coefficient, b) lift-force coefficient, c) pitching-moment coefficient, and d) lift-to-drag ratio.

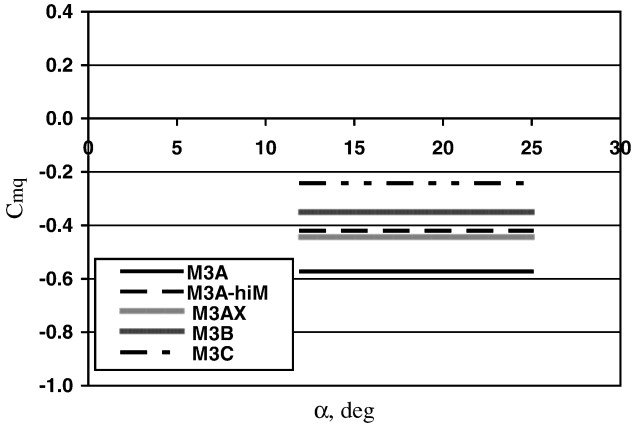

Fig. 12 Pitch-damping coefficient for tabbed (M3) geometry in supersonic flight: effects of Mach number (M3A vs M3A-hiM), axial c.g. location (M3A vs M3Ax), and radial c.g. offset (M3A, M3B, M3C).

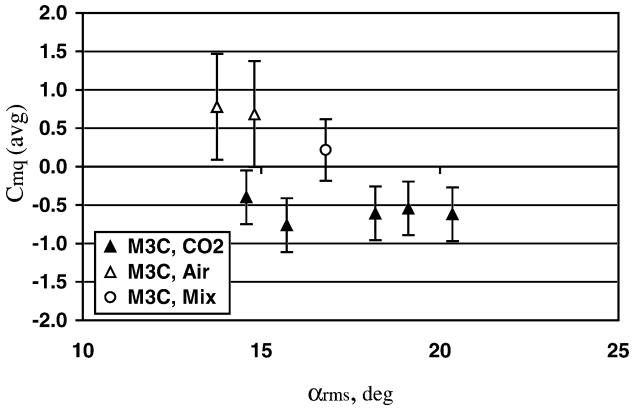

Fig. 13 Effect of test gas on pitch-damping coefficient for tabbed (M3) geometry in supersonic flight (preliminary results).

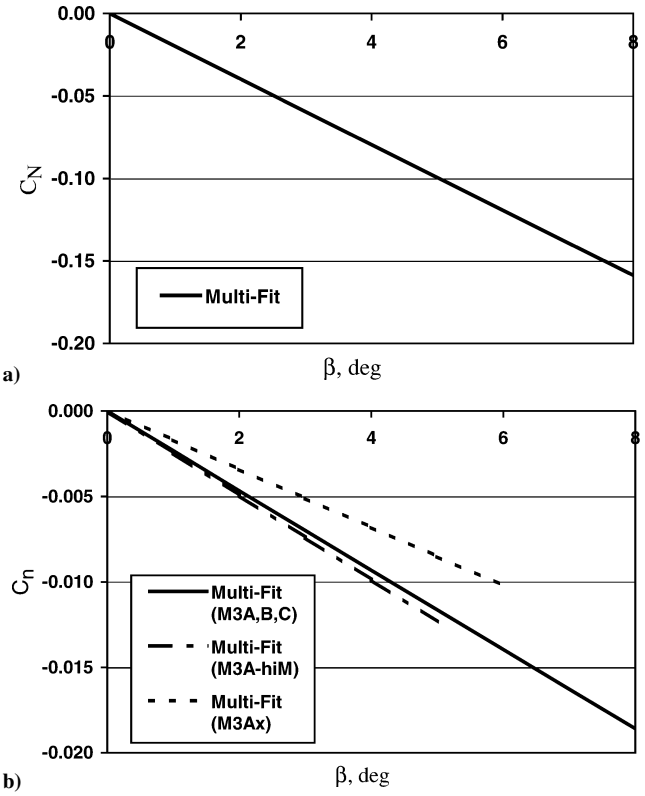

Fig. 14 Yaw-plane aerodynamics for tabbed (M3) geometry in supersonic flight: a) normal-force coefficient and b) yawing-moment coefficient.

using the quasi-linear results and are given by $0 = C_{m_0} + C_{m_\alpha}\alpha_{\text{trim}}$. For the plot in Fig. 11c, a nonlinear moment coefficient was used, and the trim angle is given by $0 = C_{m_0} + C_{m_\alpha}\alpha_{\text{trim}} + C_{m_{\alpha^3}}\alpha^3_{\text{trim}}$; the nonlinearity results in a small difference between the angles in Table 4 and those in Fig. 11c.

The errors for the tabbed configuration are larger than those for the M1 and M1A models. The primary reasons for the larger errors are 1) more information is being extracted from the data, for example, lift and side forces for the tabbed models, vs just lift for the other configurations; and 2) errors in the roll-angle measurements result in errors when separating the pitching from the yawing motion. The functions used to model the nonlinear aerodynamic coefficients are given in Eqs. (2a–2f), and the estimated values are shown in Table 5. Note, there was insufficient yawing motion during each model's flight to determine the β dependence of the drag, lift, and pitching moment, the so-called "cross terms."

The investigation of the M3's pitch damping characteristics was an important element of the ballistic range test. The results for angles close to the MSL design trim angle of attack are shown in Fig. 12. The damping coefficient was found by simultaneously reducing three to five complete test runs. Because the single-fit results indicated a nearly constant pitch damping near design trim, and there were insufficient data to extract details of the α dependence over a larger range, constant values were chosen to model the damping coefficient over the angle-of-attack range shown. The 3-σ uncertainty for the damping coefficient was on the order 0.3 for all configurations. The results show that the tabbed configuration is dynamically stable, in pitch, for all c.g. positions and both nominal Mach numbers tested. Computational predictions are not provided for pitch damping, as no CFD work was done on unsteady effects.

The ballistic range results just discussed were obtained in CO_2. However, to see if there were any gas-composition effects at the supersonic Mach numbers, two additional tests were run in air and one in a CO_2–air mixture. The results are shown in Fig. 13. It appears that the air shots were much less dynamically stable than were those in CO_2. This conclusion should be considered preliminary, as there were not enough data collected in air to justify a strong conclusion. However, the magnitude of the destabilizing pitch damping is large enough to produce a significant amplification in the angle of attack. The gas effects on the other aerodynamic parameters were very small, only 3–4%. This amount was expected based on stagnation-point pressure calculations for air and CO_2. However, the large effect of the gas composition on pitch damping was not expected, and it cannot be explained at this time.

The motion in the yaw plane was relatively small, but some information was obtained on the side-force and yawing-moment coefficients. These results are shown in Figs. 14a and 14b. The side-force coefficient is the same for all tabbed configurations, and hence only one curve is shown in Fig. 14a. However, the yawing moment depends on the axial c.g. location and, possibly, on Mach number. Therefore, the runs were divided into three groups, each with a given axial c.g. location and nominal Mach number and analyzed simultaneously within each group. The resulting multifit curves for the yawing-moment coefficients of these three groups are shown in Fig. 14b. The values of side force and yawing moment differ by small but measurable amounts from those of lift force and pitching moment. Note that because no yaw perturbations were imposed on the models, the angle range for the normal force and moment data is much smaller than it is for the pitch plane.

Conclusions

An extensive ballistic range test program, which focused on the supersonic, pitch-plane aerodynamics, in CO_2, of two candidate MSL EV geometries, in support of the MSL EV aerodynamics database, has been described. Innovative modifications to the facility and data-processing techniques were required, and implemented, to achieve successful results. One such innovation, slanting

the HFFF's powder gun, has enabled the pitch damping characteristics of moderately lifting configurations to be measured in that facility. Uncertainty (3σ) estimates for all of the static aerodynamic coefficients were determined in CO_2. Pitch-plane uncertainty estimates for the tabbed (M3) model were greater than for the axisymmetric (M1) because of the "built-in" uncertainties in yaw angle and roll rate for the former. Limited results for the M3 geometry were obtained in air and compared to those obtained in CO_2. The results imply better dynamic stability in CO_2 compared to air. This finding has not been theoretically explained. For the M1 geometry, hypersonic aerodynamic coefficients, with uncertainties, are also given. Pretest computations compared very well with the ballistic range data, providing improved confidence in CFD as a tool for experimental design. The favorable comparison also demonstrates the potential for the combination of CFD and limited, supporting experiments to produce high-quality aerodynamics databases.

Acknowledgments

The authors gratefully acknowledge the significant contributions to this work made by Chuck Cornelison, Don Holt, Don Bowling, and Rick Smythe of the Ames Research Center Hypervelocity Free Flight Facility (ARC); Jim Scott and Shawn Meszaros of the ARC Model Machining and Instrumentation Branch; Bob Bagne and Jorge Rios of the ARC Photo Lab; Bob Kruse and Bill Newby of Eloret; and Ben Ostrander of Foothill/De Anza College.

References

[1]Brauer, G. G. L., Cornick, D. E., and Stevenson, R., "Capabilities and Applications of the Program to Optimize Simulated Trajectories (POST)," NASA CR-2770, Feb. 1977.

[2]Sammonds, R. I., and Dickey, R. R., "Effectiveness of Several Control Arrangements on a Mercury-Type Capsule," NASA TMX-579, Oct. 1961.

[3]Canning, T. N., Seiff, A. , and James, C. S. (eds.), *Ballistic Range Technology*, AGARDograph 138, Aug. 1970.

[4]Intreiri, P. F., and Kirk, D. B., "High-Speed Aerodynamics of Several Blunt-Cone Configurations," *Journal of Spacecraft and Rockets*, Vol. 24, No. 2, 1987, pp. 127–132.

[5]Yates, L. A., and Venkatapathy, E., "Free-Flight Trim-Angle Predictions for the Aeroassist Flight Experiment," *Journal of Spacecraft and Rockets*, Vol 29, No. 3, 1992, pp. 335–343.

[6]*The General Aerodynamics Simulation Program (GASP) v3.0 User's Manual*, AeroSoft, Inc., Blacksburg, VA, March 1996.

[7]Haas, B. L., and Venkatapathy, E., "Mars Pathfinder Computations Including Base-Heating Predictions," AIAA Paper 95-2086, June 1995.

[8]Wercinski, P. F., Henline, W. D., Tran, H., Milos, F., Papadopoulos, P. E., Chen, Y.-K., Venkatapathy, E., and Tauber, M., "Trajectory, Aerothermal Conditions, and Thermal Protections System Mass for the Mars 2001 Aerocapture Mission," AIAA Paper 97-0472, Jan. 1997.

[9]Prabhu, D. K., Wright, M. J., Marvin, J. G., Brown, J. L., and Venkatapathy, E., "X-33 Aerothermal Design Environment Predictions: Verification and Validation," AIAA Paper 2000-2686, June 2000.

[10]Park, C., Howe, J. T., Jaffe, R. L., and Candler, G. V., "Review of Chemical-Kinetic Problems of Future NASA Missions, II: Mars Entries," *Journal of Thermophysics and Heat Transfer*, Vol. 8, No. 1, 1994, pp. 9–23.

[11]*Gridgen User Manual, Version 13*, Pointwise, Inc., Bedford, TX, Jan. 1998.

[12]Davies, C. B., and Venkatapathy, E., "SAGE, The Self-Adaptive Grid codE, Version 3," NASA TM-1999-108792, Aug. 1999.

[13]Yates, L. A., and Chapman, G. T., "Aerodynamic Ballistic Range Analysis Using Generalized Math Models," AIAA Paper 96-3360, Aug. 1996.

M. K. Lockwood
Guest Editor